Talanta 266 (2024) 125079

Contents lists available at ScienceDirect

Talanta

journal homepage: www.elsevier.com/locate/talanta

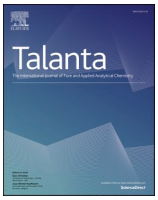

In-line Raman spectroscopy for characterization of an industrial poultry raw material stream

Tiril Aurora Lintvedt [a,b,*], Petter Vejle Andersen [a], Nils Kristian Afseth [a], Jens Petter Wold [a]

[a] Norwegian Institute for Food, Fisheries and Aquaculture Research, Muninbakken 9-13, Breivika, Tromsø, 9291, Norway
[b] Faculty of Science and Technology, Norwegian University of Life Sciences, Ås, 1432, Norway

ARTICLE INFO

Handling Editor: Joaquim Nobrega

Keywords:
Raman spectroscopy
Wide area illumination (WAI)
In-line measurements
Food characterization
Heterogeneous raw materials
Process analytical technology (PAT)

PACS:
0000, 1111 2000 MSC
0000, 1111

ABSTRACT

In this work, we evaluated the feasibility of Raman spectroscopy as an in-line raw material characterization tool for industrial process control of the hydrolysis of poultry rest raw material. We established calibrations (N = 59) for fat, protein, ash (proxy for bone) and hydroxyproline (proxy for collagen) in ground poultry rest raw material. Calibrations were established in the laboratory using poultry samples with high compositional variation. Samples were measured using a wide area illumination Raman probe at varying working distance (6 cm, 9 cm, 12 cm) and probe tilt angle (0°, 30°) to mimic expected in-line variations in the measurement situation. These moderate variations did not significantly affect performance for any analytes. The obtained calibrations were tested in-line with continuous measurements of the ground poultry by-product stream at a commercial hydrolysis facility over the course of two days. Measurements were acquired under demanding conditions, e.g. large variations in working distance. Reasonable estimates of compositional trends were obtained. Validation samples (N = 19) were also reasonably well predicted, with $RMSEP_{corr}$ = [0.14, 1.37, 2.36, 1.51]% for hydroxyproline, protein, fat and ash, respectively. However, there were indications that further calibration development and robustification of pre-processing would be advantageous, particularly with respect to hydroxyproline and protein models. It is the authors' impression that with such efforts, potentially in combination with development of practical measurement setup, the use of Raman spectroscopy as a process control tool for the hydrolysis of poultry rest raw materials is within reach.

1. Introduction

In recent years, the poultry processing industry have adopted enzymatic protein hydrolysis (EPH) as a strategy to recover constituents from by-products (e.g. carcasses and mechanical deboning residues). In this process, proteins from the by-products are digested and solubilized by proteases. After hydrolysis, the enzyme is inactivated at near-boiling temperatures and the slurry goes into a separator, from which three fractions are recovered; a peptide water phase (i.e. protein hydrolysate), an oil phase and a low value collagen-and-mineral rich solid residue.

Today, recovered constituents from EPH usually end up as lower value feed ingredients (used for e.g. pet food), and for such processes maximising the protein yield is of major importance. In recent years, however, the focus has been shifting towards protein ingredients for higher-paying markets like human consumption. This puts increasing emphasis on protein quality (e.g. producing protein hydrolysates with specific functional or nutritional properties), and not only on protein recovery. The raw materials entering the hydrolysis process are typically very heterogeneous, consisting of different mixes of e.g. water, meat, skin, tendons and bone from chicken and turkey. This variation is a challenge when specific and stable product quality is important. It has been found that poultry raw material variation impacts quality parameters such as peptide size distribution and amino acid composition [1]. Furthermore, the product quality is a function of raw material quality in combination with different process parameters. For instance, collageneous proteins are harder to solubilize than muscle proteins and might require different process settings [2]. Therefore, Wubshet et al. [3] reported a proof-of-concept feed-forward setup, where end-product characteristics (protein yield and average molecular weight) were predicted based on spectroscopic measurements of the raw material in combination with hydrolysis time. They obtained $R^2 = 0.88$ for protein yield and $R^2 = 0.56$ for average molecular weight. These findings illustrate that characterization of the input material has potential to be used in process control for optimization of yield and product quality.

* Corresponding author. Norwegian Institute for Food, Fisheries and Aquaculture Research, Muninbakken 9-13, Breivika, Tromsø, 9291, Norway.
E-mail address: tiril.lintvedt@nofima.no (T.A. Lintvedt).

https://doi.org/10.1016/j.talanta.2023.125079
Received 8 March 2023; Received in revised form 4 August 2023; Accepted 13 August 2023
Available online 19 August 2023

Near-Infrared spectroscopy (NIRS) is a well-established technique for in-line compositional analysis of foods. The technique is particularly suited for estimation of the gross components in foods, such as fat, water and protein. However, NIRS has clear limitations when it comes to detailed compositional analysis, meaning that targeting detailed chemistry like protein composition can be challenging [4]. Moreover, NIRS models can seldom be transferred directly from laboratory calibration to industry without recalibration or calibration transfer methods. Physical differences between laboratory and industry samples and sampling situation usually lead to large biases [5,6]. This makes the calibration development and practical application labour intensive. Raman spectroscopy, on the other hand, is a technique that might ease some of these challenges. Raman spectroscopy is a promising spectroscopic technique for in-line food analysis, with the advantage that both gross components, including fat [7], proteins [7] and bone [8,9], can be targeted at the same time as more detailed information on protein composition, e.g. the concentration of collagen [4]. In general, recent work have indicated that Raman might be more robust with respect to tackling sample variation than NIRS [10,11], due to more unique and non-overlapping analyte fingerprints.

A main limitation for in-line compositional analysis with Raman spectroscopy for a heterogeneous raw material stream, is the small sampling volume obtained with the laser. By using Wide Area Illumination (WAI) probes, the laser spot is widened (3–6 mm diameter) compared to traditional Raman probes, which is an advantage when aiming to cover the surface of more heterogeneous materials. As reviewed by Shin and Chung [12], the WAI probes can improve the accuracy of Raman spectroscopic analysis for a variety of heterogeneous samples (e.g. in the pharmaceutical, polymer and agricultural domains) due to their effective enhancement in sample representation (surface area and depth) and reproducibility in the spectral collection. Using such a probe, Lintvedt et al. [9] scanned heterogeneous and homogenized poultry samples and found that the estimation of ash from the two sample versions gave similar performance. This showed that employment of WAI Raman probes are promising with respect to robust measurements of heterogeneous streams of poultry by-products. For in-line measurements, variations in working distance is expected in addition to heterogeneity. Other studies [13,14] have shown that the WAI Raman probes are good alternatives to traditional Raman probes when moderate variations in working distance are expected. This is because the WAI Raman probes do not employ strongly focused lasers. Although studies have indicated that moderate variations in working distance impact spectrum intensity less for WAI probes, the critical variation in working distance will most likely depend on the pre-processing of spectra, material properties and the analyte of interest. This motivates a study on how variation in working distance affects the estimation of fat, protein, bone and collagen in ground poultry rest raw material.

The main aim of the present study was to use in-line Raman spectroscopy for characterisation of an industrial poultry raw material stream. In the work, calibrations based on Raman measurements of fat, protein, ash (proxy for bone) and hydroxyproline (HYP, proxy for collagen) in ground poultry rest raw material were established. All samples were measured using a WAI Raman probe at varying working distance (6 cm, 9 cm, 12 cm) and probe tilt angles (0°, 30°) to mimic expected in-line variations. All calibrations were based on sample designs with high chemical variation measured in a laboratory environment. Subsequently, the obtained calibrations were tested for continuous monitoring of a ground poultry by-product stream at a commercial hydrolysis facility over the course of two days. To the best of our knowledge, this is the first time a WAI Raman probe has been tested in-line under relevant measurement conditions in the food industry.

2. Material and methods

2.1. Sample materials

Calibrations (N = 59) were made based on 49 designed samples and 10 samples acquired directly from the input stream of a commercial hydrolysis process (Bioco, Hærland, Norway). For the process samples, the mix ratio of two separate input streams for turkey and chicken were varied in the range of 100% chicken - 25% chicken. The designed calibration samples were based on a variety of raw materials acquired from the associated poultry processing plant (Nortura, Hærland, Norway). The samples were made by mixing the following ground base materials,

A: Mechanical deboning residues from chicken by-products
B: Chicken by-products prior to mechanical deboning
C: Turkey by-products prior to mechanical deboning
D: Mechanically deboned chicken meat
E: Chicken fillet
F: Chicken skin
G: Approximately 60% material D and 40% tap water
H: Tendons and skin

Mechanical deboning is a process where the remaining meat on the carcasses after filleting is separated from the bones, resulting in two fractions: The mechanically deboned meat, containing mostly meat, and the mechanical deboning residues containing more bone. The batches of chicken skin (F) and tendon-skin-mix (H) were difficult to grind fresh and were frozen before being ground. All other base materials were taken from the process line and vacuum packed in smaller bags to keep as fresh as possible throughout the 3 experiment days. Each calibration sample was made by mixing six sub-samples of the available base blends A-H in shares according to the sample design (See section 2.2 and Tab. A.2). The samples were made consecutively during the experiment and the base blends were kept in a cold room (0–4 °C) throughout the whole experiment. Measurements of the samples were done in room temperature.

A validation set (N = 19) was obtained based on samples acquired from the commercial process during in-line measurements at the hydrolysis facility. Six of the samples were made by adding other materials, which could be relevant for long-term variation, manually to the grinder. These materials were acquired from the poultry production line at Nortura, and corresponded with material groups C, B, F mixed with the in-line stream and finally C mixed with in-line stream. The sampling was done with help of a half-cylinder tool, which allowed measurements to be done on the material simultaneously with the sampling. This resulted in a large sampling volume, from which the illuminated surface layer was collected (ca 300–500 g). The samples were immediately vacuum packed and frozen. Later, the samples were half thawed and homogenized to be measured again under controlled conditions in the laboratory.

2.2. Calibration sample design

The target analytes fat, protein, HYP and ash content may typically covary in this kind of material. To reduce these correlations and to elucidate how independently we could model the different analytes, we carefully designed the sample set. Prior knowledge of the approximate composition of each base materials (A-H) were found from previous analyses on similar samples or in the literature and used to estimate expected sample composition of all possible mixes of the eight base materials. From the candidate samples, 49 samples were selected using the Kennard-Stone algorithm to obtain samples with large variation and low covariance between the analytes. Water was added in material G to introduce samples with lower concentrations of both fat and protein, in order to break covariances between these two analytes in the sample set. The final sample design is provided in Tab.A.2.

2.3. Measurements and data analysis

2.3.1. Raman measurements for calibration set

A MarqMetrix All-in-One (AIO) Raman system covering a Raman shift range of 100–3250 cm^{-1} was employed for all Raman measurements. The system was equipped with a 785 nm laser operating at 450 mW power and the sampling optic was a wide area illumination (D = 3 mm) Proximal BallProbe HV stand-off Raman probe (MarqMetrix Inc., Seattle, WA, USA). Calibration samples were measured in the laboratory. Samples were placed in a rectangular aluminum sample holder (20 cm × 15 cm × 2 cm). The surface of each sample were scanned with the Raman probe, accumulating a signal with a 6s x 5 exposure time, as illustrated in Fig. 1. This exposure time was chosen to obtain sufficient signal-to-noise ratio (SNR), while avoiding signal saturation. Since the ultimate goal was to measure a continuous stream, the exact choice of number of averages (i.e. total exposure time) was not strongly restricted by the practicalities of the upcoming in-line measurements. To mimic variations in the measurement situation that can be expected to occur in a real raw material stream, we measured all samples at a working distance of 6, 9 and 12 cm. For the optimum working distance of 9 cm, we also acquired measurements with a 30° tilt of the Raman probe (Fig. 1). Three replicate measurements were acquired for each measurement setup.

2.3.2. Raman measurements for validation set

Continuous in-line measurements for testing of the laboratory calibrations were done at the poultry hydrolysis facility over 2 days. The Raman probe was placed at the outlet of a grinder, i.e. at the input stream to the hydrolysis process. Fig. 1c shows the hydrolysis process as well as the Raman measurement location. Photos and videos from the measurement location are shown in Fig.C.9 and the Supplementary Material, respectively. The probe was placed at a working distance of approximately 8 cm when the output stream was at maximum. However, the working distance varied in correspondence with the output volume, alternating from maximum stream and optimal working distance to no stream at all. This certainly affected the quality of the collected spectra, and a method for filtering out low quality spectra was needed.

Different exposure times from those used during calibration was employed in-line. This was due to the alternating grinding which provided a maximum output volume only for a limited time. The exposure time for each spectrum was set to 6s x 2 on the first day. It was adjusted to 5s x 3 on the second day to avoid saturation of the detector due to higher fluorescence levels from the material. A dark measurement was acquired approximately every 30 min. The software Aspen Process Pulse (Aspen Technology Inc., Bedford, MA, USA) was used for real-time analysis of the analytes. Later, the acquired samples were measured again under controlled conditions in the laboratory employing a working distance of 9 cm and an exposure time of 4s x 10, with the same scanning strategy as illustrated in Fig. 1a. The further decrease in exposure time compared to previous measurements was needed due to increased fluorescence associated with sample degradation.

2.3.3. Reference measurements

Samples taken directly from the input stream to the hydrolysis were quite coarse and were therefore homogenized before reference analyses. The samples were first frozen at −20 °C and homogenized in half frozen state (10000 RPM for 6s × 4). Reference analyses were carried out at an external laboratory (ALS Laboratory Group, Oslo, Norway). Determination of ash concentration (% of wet weight) were carried out by gravimetric analysis (BS 4401 Part1 1998 Commision Regulation (EC) 152/2009 MU 6.5%). Fat concentrations (percent of wet weight) were determined by pulsed NMR analysis (MU 6.5%). HYP concentrations (% of wet weight) were determined by oxidizing HYP using chloramine T and subsequently producing chromophores by the product's reaction with 4-dimethylaminobenzaldehyde (based on BS 4401–11:1995). The chromophores were measured spectrophotometrically and finally compared with standard HYP solutions. Protein concentrations (% of wet weight) were estimated from the nitrogen content using a conversion factor of 6.25. Nitrogen was determined by complete combustion of the sample in the presence of oxygen.

2.3.4. Pre-processing of spectral data

The Raman shift range 520–1800 cm^{-1} was used in the data analyses. Cosmic ray spikes were removed by a simple spike detection algorithm based on derivatives. Subsequently Savitsky-Golay (SG) smoothing (polynomial order 2 and window size 9) [15] was applied, and a baseline correction was done by the Asymmetric Least Squares (ALS) algorithm [16,17]. The baseline correction employed a smoothing parameter of 4 and an asymmetric weighting parameter (of the residuals) of 0.01. Finally, each spectrum was normalized by the intensity of the sapphire peak at 750 cm^{-1}, mainly with the aim to correct for intensity variations due to varying working distances or potential laser fluctuations. The sapphire signal originates from the sapphire in the probe optics.

2.3.5. Data modeling

Partial least squares regression (PLSR) [18,19] was used for model development. For the calibration set, separate models were made for the different combinations of working distance and probe tilt. The separate models were compared with a combined data set which included all measurement variations. To establish whether the estimation errors acquired were significantly different, cross validation (CV) together with a three-way analysis of variance (ANOVA) of the squared residuals (unbalanced design) was employed, as adapted from Indahl and Næs [20]. The factors included were the sample number, the calibration model and the measurement setup. In the CV, one sample was held out at a time, with all replicate measurements included in the same segment to avoid overfitting. Predictions based on the replicate measurements of each sample were treated separately during calculation of the performance metrics. A simple criterion using a 4% punish factor, as described

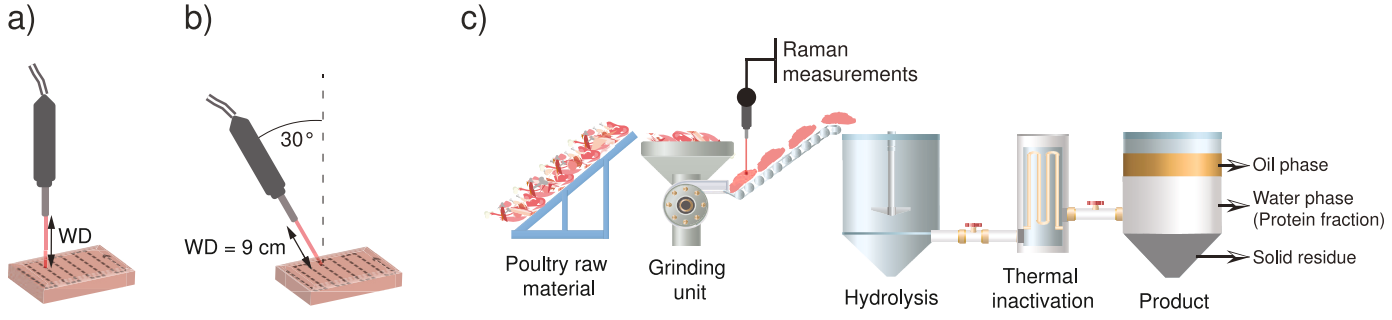

Fig. 1. Laboratory measurement setup for calibration samples, illustrating the usual backscattering setup for which we acquired measurements at varying working distances (WD) (a) and the probe tilt setup measured at a 9 cm working distance (b). These variations are meant to mimick varying in-line measurement conditions. A schematic illustration of the hydrolysis process, with the in-line Raman measurement location indicated is shown (c). Adapted from Wubshet et al. [3].

by Westad and Martens [21], was used to determine the number of components for the calibration models. For the in-line testing, the calibrations based on all working distances and probe tilts were used. Due to light pollution from an LCD computer screen used during the experiment, some regions in the in-line spectra had to be removed from the calibration, including 628–648, 832–852, 862–880, 994–1010, 1769–1788 cm^{-1}. During process use, there is no need for this LCD screen close to the in-line Raman setup. For the calibration, we report performance through the coefficient of determination (R^2) and the root mean squared error (RMSE). For the in-line and laboratory validation, we also report these metrics when corrected for slope and bias errors, to emphasize what performance could be achieved if the cause of these errors is identified and corrected for.

2.3.6. Filtering of low quality in-line spectra

To remove in-line spectra acquired when there were little to no output stream at the grinder (i.e. large working distance) and spectra that were close to detector saturation, spectra with low SNR were filtered out. For calculating the SNR, the spectra were first pre-processed as described in section 2.3.4. Then, the SNR of each spectrum was calculated as the ratio between the average spectrum intensity and the standard deviation of the estimated noise, according to Eq. (1).

$$SNR = \frac{mean(I)}{sd(I_n)}, \tag{1}$$

where I is the spectrum intensity and I_n is the estimated noise intensity. Noise was estimated by subtracting a smoothed version of the spectrum from the original spectrum. For smoothing we used SG with polynomial order 2 and window size 9. This is similar to Guo et al. [22] and same as in previous work [9]. Spectra with SNR lower than 23 were discarded. This threshold was chosen so that all validation sample spectra could be categorized of sufficient quality, since large working distances were not expected during sampling.

3. Results and discussion

3.1. Sample variation

An overview of sample variations and analyte correlations in the calibration and validation set can be found in the appendix (Fig.A.7). The calibration samples had large variations in chemistry: 1) HYP: 0.1–1.3%, 2) Water: 51–76%, 3) Protein: 10–22%, 4) Fat: 2–37% and 5) Ash: 0.5–6.2%. Several of the design samples could be considered extreme with respect to expected in-line variations. For instance, several samples contained mainly skin (very high fat) while others consisted mainly of the tendons-skin mix or chicken fillets only. Although an aim was to include large variations in composition while keeping the covariance between the different analytes at a minimum, some analytes still had considerable correlations. Fat and protein concentrations had the highest correlation ($r = -0.73$), followed by HYP and ash ($r = 0.42$). The tendon-skin samples were important to break correlations between ash and HYP (the correlation increased to $r = 0.75$ when they were not included). The extreme skin and fillet samples were the main reason why the correlation between fat and protein was still considerable. When removing the most high-fat and high-protein samples ($y_{fat} > 25\%$ and $y_{protein} > 18\%$) correlation could be reduced to $r = -0.33$. However, this led to an increased correlation between protein and ash ($r = 0.48$). As a high degree of heterogeneity of material should be expected in-line over time and be accounted for, we chose to not remove any extreme samples from the main analyses in this work. However, it is important to note that this did indeed impact the calibration set correlations and could impact model robustness.

With respect to the validation samples acquired in-line, a reasonable variation in most analytes were obtained (Fig.A.7), partially thanks to the manual addition of extra material. Interestingly, the variation in HYP concentration covered a different range compared to the calibration set, i.e. lacking the low concentrations. The variation in ash concentration was moderate (3–6%), with the exception of one sample at approx 13%.

3.2. Spectral features

Fig. 2 shows spectra from each of the 8 base materials used in the calibration sample design. There were clear differences in the spectral fingerprints. Material E (chicken fillets) mainly exhibit spectral features associated with protein, while material F (skin) mainly shows spectral features associated with lipids. Material A has high bone (ash) content and material H has high collagen (HYP) content. Important Raman active groups associated with lipids include the out-of-phase aliphatic C–C stretch (1064 cm^{-1}), the liquid aliphatic C–C stretch in gauche (1080 cm^{-1}), the methylene twisting deformation (1301 cm^{-1}), the methylene scissor deformation (1440 cm^{-1}), the in-plane cis olefinic hydrogen bend (1267 cm^{-1}) and the cis olefinic stretch (1657 cm^{-1}) [23,24]. As Fig. 2 suggests, several bands associated with protein overlap with lipid related bands, for example the C–H deformation (1450 cm^{-1}), the Amide I (1657 cm^{-1}) and the Amide III (1250, 1270 cm^{-1}) [25]. Other notable bands associated with proteins originate from phenylalanine (1002 cm^{-1}), tryptophan (958, 1342, 1555 cm^{-1}), tyrosine (641, 829, 856 cm^{-1}), peptide C–N bonds (1125 cm^{-1}), peptide backbone $N - C_\alpha - C$ (936 cm^{-1}) and disulfide bonds (532 cm^{-1}) [25]. With respect to bone content, the main Raman band of interest was found at 960 cm^{-1}, which is associated with phosphate. The importance of this band originates from the high correlation between ash and calcium, since calcium is a major bone mineral and exists mainly as a phosphate salt [8]. In addition to the analytes of interest, some of the apparent peaks are also associated with instrumental components, such as the sapphire in the optics (e.g. 750 cm^{-1}). The recorded background spectrum is shown in Fig.B.8.

3.3. Calibration

3.3.1. Regression models

Fig. 3 shows the regression results and the regression coefficients obtained for the different analytes. Here, spectra from all working distances and probe tilts were included in a single calibration for each analyte. Overall, the performance was high for all analytes ($R^2_{CV} > 0.8$). The ash model was dominated by the 960 cm^{-1} phosphate band, but included a weaker negative weighting of the 1657 band, associated with fat. This corresponded to the moderate negative correlation between fat and ash seen in the calibration set. Similar regression coefficients have been obtained in previously published work [8]. The fat model had a low degree of complexity (LV = 3) and exhibited expected features, consisting mainly of positive weighting of bands associated with lipids (1080, 1306, 1437, 1655 cm^{-1}) and negative weighting of bands associated with protein (e.g. 940, 1129 cm^{-1}). The model was dominated by bands related with saturated fat, as seen by the strong weighting of saturated modes (1080, 1306, 1437 cm^{-1}) and weaker weighting of unsaturated modes (1267, 1655 cm^{-1}). This was reasonable since a majority of the fat in these samples is saturated. The protein model was more complex (LV = 7), but the model corresponded well with expectations. The main positively weighted bands are associated with the disulfide bonds (528 cm^{-1}), tyrosine (823, 854 cm^{-1}), the peptide backbone $N - C_\alpha - C$ (936 cm^{-1}), tryptophan (958, 1340, 1555 cm^{-1}), phenylalanine (1002 cm^{-1}), the peptide C–N bonds (1127 cm^{-1}), and C–H deformation (1454, 1466 cm^{-1}) [25]. The main negatively weighted regions were associated with lipids (1266, 1302, 1442, 1659 cm^{-1}) and this indirect modelling was most likely a consequence of the considerable negative correlation between fat and protein in the calibration set. The correlation between HYP and protein was low, and the HYP model was clearly different from the total protein model,

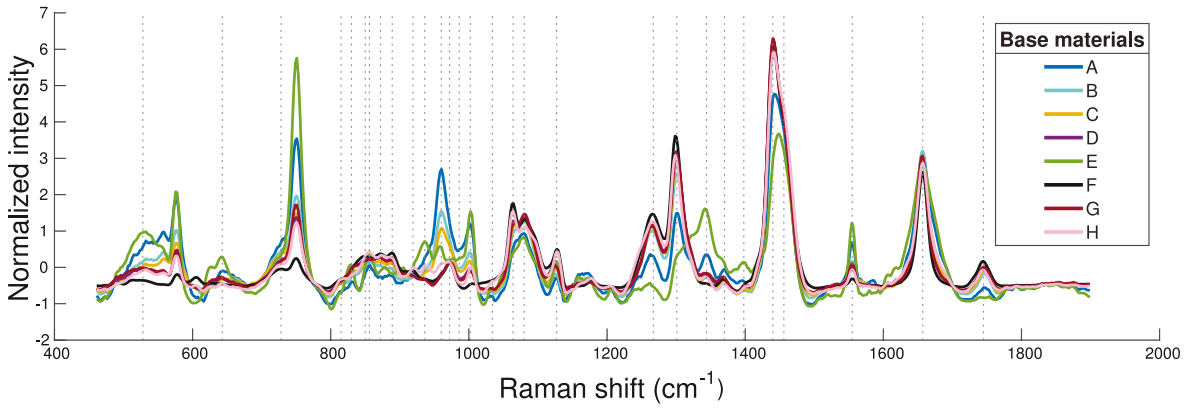

Fig. 2. Baseline corrected and normalized (SNV) spectra from the 8 different poultry base materials used in the designed calibration samples, elucidating the difference in their spectral signatures. Important peaks and shoulders are indicated (dashed lines). The apparently large variation in the sapphire peak at 750 cm^{-1} is mainly an effect of the normalization procedure applied here for illustration purposes.

emphasizing the uniqueness of the HYP spectral fingerprint from other proteins. The main differences from the protein model were the relatively stronger weighting of the Amide I component at 1678 cm^{-1}), the weaker weighting of the C–N band at 1129 cm^{-1} and tryptophan (indole ring) at 1555 cm^{-1} and the relatively stronger weight of the peptide backbone component at 919 cm^{-1} ($N - C_{\alpha} - C$). These observations are in accordance with characteristics for collagens [25]. A relatively stronger weight of the amide III band (1245 cm^{-1}) compared to the protein model was also found. Another interesting observation was that while protein models weighted the tyrosine doublet (827, 856 cm^{-1}) positively, the HYP models weighted the 827 cm^{-1} band negatively and the 856 cm^{-1} band positively, indicating the importance of the ratio between exposed and buried tyrosine. Overall, the obtained regression coefficients corresponded well with previous work on similar material [4].

3.3.2. *Implication of moderate variations in measurement situation*

Cross validated regression models based on Raman measurements employing different working distances and probe tilts, are shown in Table 1. The performance based on the model with all measurement setups merged was not significantly ($\alpha = 10\%$) different from the performance of models based on separate measurement setups, for any analytes. This demonstrated that the WAI Raman probe tackled moderate variations in working distance and probe tilt well. However, while the fat models had a stable number of components suggested across all measurement setups, the other analytes had more variations. This could indicate that the fat model was less influenced by variation in measurement situation than HYP, protein and ash models. Moreover, fat is the analyte largely dominating the overall Raman signals in the spectra (due to a combined Raman scattering efficiency and concentration effect). This could also therefore explain the effects seen in the table. Interestingly, the set including all variations in measurement setups consistently suggested the highest number of components. This could either indicate an increased complexity to compensate for effects of varying working distance or simply that employing this many components might be overfitting.

Our hypothesis was that normalization by the sapphire peak should correct for intensity differences as a function of working distance. Indeed, the SNR and average normalized spectrum intensity was little affected by the moderate variations in working distance, with SNR between 45 and 48 and average intensity between 0.30 and 0.31. However, the effect was moderate even when omitting the normalization, which showed that the WAI probe itself tackled the variations in working distance well. Hence, the mentioned hypothesis was not properly tested during these lab calibrations. However, when this normalization was omitted, a strong negative regression coefficient for the sapphire peak was produced for all analytes (except HYP). Although this only moderately impacted the performances, it greatly altered the regression coefficients. Although the negative weighting was stronger for the set combining measurements of different working distances, it was still present in varying degrees also for the other sets where working distances were constant. This showed that there might be other factors influencing the sapphire peak as well, and that further elucidation of this normalization strategy is of interest.

3.4. *In-line validation*

3.4.1. *Model adjustments*

As discussed in section 3.3.1, the regression coefficients acquired for the cross-validated calibrations represented models which corresponded well with literature. However, for the validation samples, employing models of the suggested complexity did not provide optimal results. The number of latent variables employed in the PLSR were instead decided based on a criteria that slope should be close to 1 and that the RMSEP corrected for slope-and-bias errors should be as low as possible. Fig.C.12 shows the regression coefficients that were employed, both for the in-line measurements and the control laboratory measurements. For the fat models, the number of components was unchanged in both cases, again emphasizing the stability and robustness of these models. For ash, a moderate decrease from 5 to 4 components was observed in both cases, indicating slight overfitting in the calibration set. The number of LVs were more critically adjusted for HYP and protein models. The number of LVs in the protein model was decreased from 7 to 2-and-3, respectively. The main effect of this was stronger indirect modelling on bands associated with other analytes, i.e fat and ash. For the in-line HYP model, the number of LVs were reduced from 7 to 3 and overall became more similar to the protein models. This was not the case for the HYP model based on controlled laboratory measurements, which only had a moderate decrease from 7 to 6 LVs.

Several factors might have contributed to the model changes that were observed between the calibration and validation set as well as the discrepancies between the in-line and laboratory models. Overfitting of the calibration set might be one factor, but another important factor was the light pollution from the LCD computer screen during in-line measurements. The signals consisted of narrow peaks which varied in intensity and resulted in mismatches in the dark subtraction, and the corresponding regions needed to be discarded. This had little effect on the fat and ash models, as the regions did not correspond to any important bands associated with these analytes. The protein and HYP models were more affected, as the discarded regions were associated with e.g. phenylalanine (994–1010 cm^{-1}), tyrosine (832–852, 862–880 cm^{-1}) and tryptophan (862–880 cm^{-1} cm^{-1}). The choice of number of

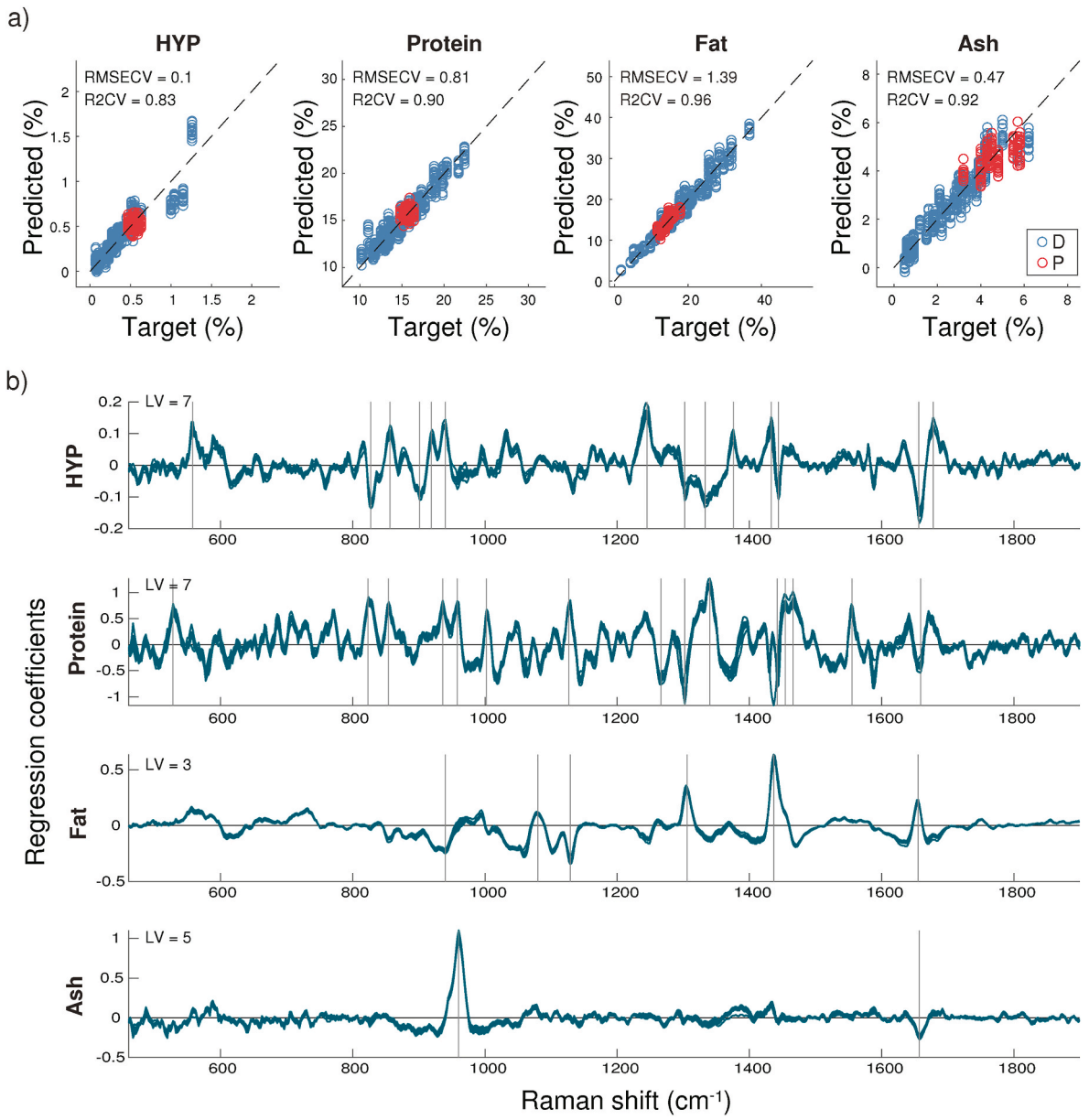

Fig. 3. Predicted versus target values (a) for the calibration set including measurements in all working distances and probe tilts, with corresponding regression vectors for fat, protein, ash and HYP (b). Important regions are marked (lines). The number of latent variables (LV) employed in the respective PLSR models is indicated. Distinction is made between the design (D) and process (P) calibration samples.

Table 1
Cross validated PLSR performance for fat, protein, ash and HYP estimation, using the calibration samples and varying measurement setups.

Measurement setup		Performance											
WD[a]	Tilt angle	HYP			Protein			Fat			Ash		
		$RMSE_{CV}$	R^2_{CV}	LV[b]	$RMSE_{CV}$	R^2_{CV}	LV	$RMSE_{CV}$	R^2_{CV}	LV	$RMSE_{CV}$	R^2_{CV}	LV
6 cm	0°	0.12	0.78	5	0.85	0.89	4	1.29	0.97	3	0.50	0.91	2
9 cm	0°	0.11	0.81	7	0.88	0.89	4	1.30	0.96	3	0.48	0.92	5
9 cm	30°	0.10	0.83	6	0.79	0.91	6	1.34	0.96	3	0.48	0.92	5
12 cm	0°	0.11	0.80	5	0.71	0.93	7	1.39	0.96	3	0.50	0.91	4
all	all	0.10	0.83	7	0.81	0.91	7	1.39	0.96	3	0.47	0.92	5

[a] working distance.
[b] number of latent variables employed in the PLS model.

LVs for the controlled laboratory measurements could potentially also be affected by the homogenization of the samples.

3.4.2. *Filtering out low quality spectra*

Fig. 4a shows the in-line spectra that were filtered out by the SNR thresholding routine. The low quality spectra included many low

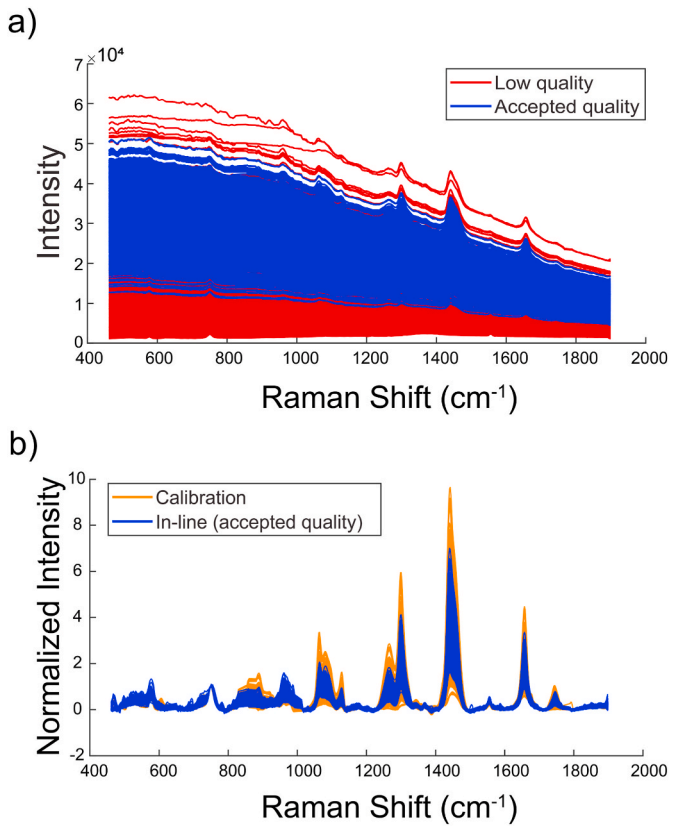

Fig. 4. All raw spectra acquired in-line at the hydrolysis plant, showing low quality spectra which were filtered out and the spectra with sufficient quality used for predictions (a) and the pre-processed version of the accepted spectra compared to calibration spectra (b).

intensity spectra corresponding to large working distances or no material stream at the grinder. A few high intensity spectra were also filtered out, due to strong fluorescence that lead to a large shot noise component combined with near-saturation effects. The in-line variations in working distances were much larger (ca 4–30 cm) than accounted for in the calibration (6–12 cm). There was still a large range of intensities among the accepted spectra (Fig. 4a and b). This could potentially be explained by chemistry alone, but could also potentially be related to working distance intensity fluctuations not accounted for by the sapphire normalization.

The filtering routine was based on a simple thresholding of the spectrum SNR. In the calibration set, the SNR and average spectrum intensity was little affected by the moderate variations in working distance. Since the variations were much larger during in-line measurements, the SNR did vary with the alternating working distance (Fig. C.10). However, the SNR could also be influenced by other phenomena that changes either the average Raman signal intensity (e.g. chemistry) or the noise level (e.g. shot noise from fluorescence). For example, a high fat sample measured at a large working distance could yield similar SNR as a low fat sample measured at shorter working distance. Therefore, this method might not be the best choice if one wants to specifically diagnose and filter out spectra with large working distances. Overall, further elucidation of specific spectral diagnosis and sapphire normalization dependence on working distance is of high interest.

3.4.3. Predictions

After filtering out low SNR spectra, predictions of all analytes were performed, and considerable variations around the average trend line were still present in predictions (Fig.C.11). These variations are most likely real and first of all a consequence of heterogeneity of the material stream. Identifying the main trends in material composition is the most interesting with respect to process control, as one set of hydrolysis settings would be applied to a large volume of material. The hydrolysis of the material typically runs for 45 min, and potential process adjustments based on material composition should be made within this time frame. In that regard the variations in predictions over a smaller time interval (e.g. 5 min) might not be critical for process control. By employing a 15 min moving average, temporal variations in the predicted material composition was evident (Fig. 5). By comparing the qualitative trends, expected patterns were observed. For instance higher fat concentrations were often accompanied by lower concentrations in other analytes. Around time index 800–850 (day 2), a sudden change in predicted protein, fat and ash concentration was observed, which corresponded with the extra materials that were added manually. The correlations between the predicted analyte trends corresponded well with the measured values for validation samples in case of fat-protein ($r_{val} = -0.56, r_{pred} = -0.56$), protein-hyp ($r_{val} = 0.4, r_{pred} = 0.34$) and ash-fat ($r_{val} = -0.33, r_{pred} = -0.17$). As expected due to the larger adjustments in the HYP and protein models, discussed in section 3.4.1, the HYP and protein correlations with other analytes were higher, i.e between fat-HYP ($r_{val} = -0.04, r_{pred} = 0.56$), ash-HYP ($r_{val} = 0.5, r_{pred} = 0.61$) and protein-ash ($r_{val} = 0.31, r_{pred} = 0.8$) Although HYP and protein models exhibited a larger degree of indirect modelling on fat and bone than wanted, the overall prediction trends indicated that we were able to measure chemistry in spite of the challenging measurement conditions.

3.4.4. Performance for validation samples

Fig. 6 shows the predicted versus measured values of the validation samples measured in-line and later in the laboratory. Overall, there was a certain degree of bias and slope errors for most analytes, but they were not extreme. Such errors are common when transferring models from the laboratory to industry and could be tackled by simple calibration transfer routines. Assuming these systematic errors can be resolved, the corrected prediction errors ($RMSEP_{corr}$) were still overall larger than for

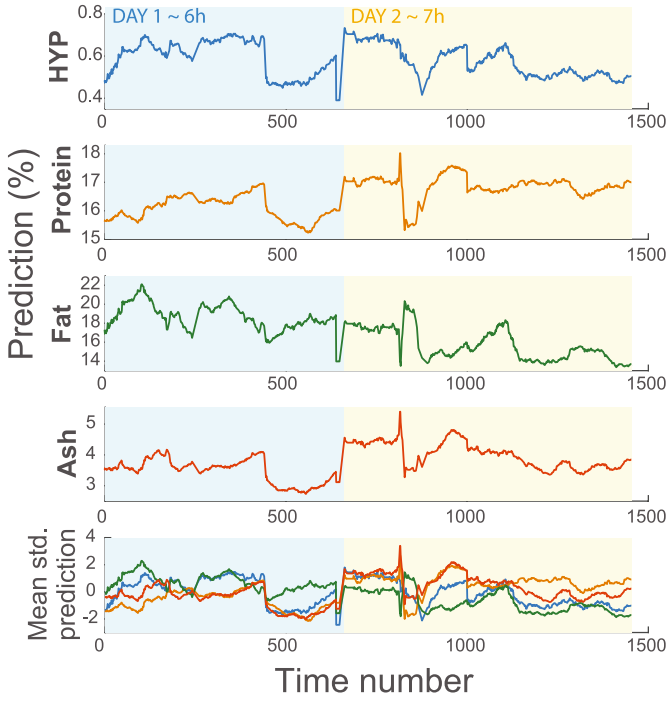

Fig. 5. Predicted trends over the two measurement days for HYP, protein, fat and ash (a–d) and the mean standardized predictions of these compounds for better comparison of qualitative trends (e). The trends are calculated as a 15 min moving average.

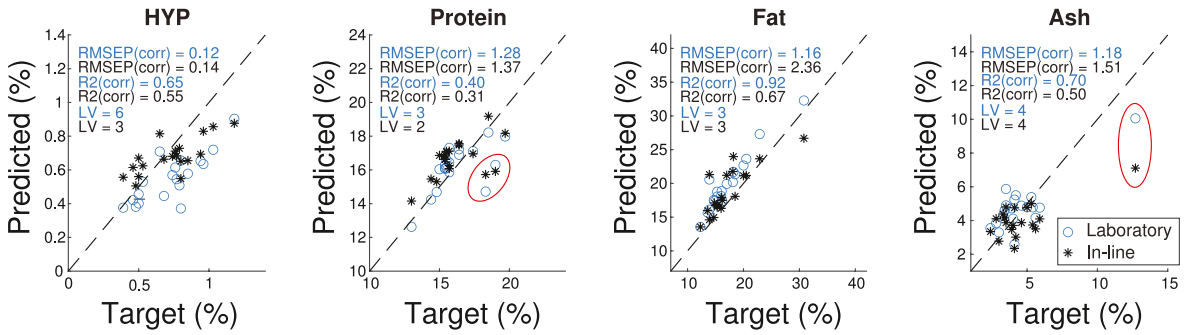

Fig. 6. Predicted versus target values for each analyte, using in-line measurements (black) and laboratory measurements (blue). Note that the reported performance metrics values are corrected for bias-and-slope errors, while the plotted predicted values themselves are not corrected. Predictions for samples which are discussed in the text are marked (red circle).

the cross-validated calibration set. One source of error for the in-line measurement was the sampling. Since the collected samples were large and the illumination area small, the spectra-to-reference correspondence was likely poorer compared to the control laboratory measurements. This was probably part of the reason why the corrected prediction errors were generally smaller for the controlled laboratory measurements. It also explains why the one sample with high ash concentration was considerably better predicted from the laboratory measurement (Fig. 6), as this sample was collected under demanding sampling conditions. For the in-line measurement implementation, heterogeneity of the raw material stream would be tackled by averaging measurements over a longer time frame. This would likely reduce sampling errors, as has been achieved for e.g. on-line measurements of fat in beef trimmings by NIR imaging [26]. As discussed in section 3.4.3, averaging would also be the preferred method in a hydrolysis process.

Although the corrected prediction errors were smaller for the laboratory measurements, there were similar bias and slope errors as for the in-line measurements, indicating weaknesses in the calibration models. This was, as discussed, particularly expected for protein and HYP models. For instance, the same two samples were underestimated with respect to protein concentration (Fig. 6) in both cases. In particular the protein predictions were affected by variations in fat concentrations, as was evident from the increased correlation between predicted protein and fat concentrations ($r_{inline} = -0.76$) compared to the true values ($r = -0.56$). This revealed robustness issues, i.e dependence on conserved correlations with fat, which was not clear from the predictions over the full time span discussed in section 3.4.3. The HYP performance mainly had bias and slope issues, while the $RMSEP_{corr}$ was similar to those obtained in the calibration set. The former errors could be related to the lack of samples with moderate-to-high HYP concentrations in the calibration set. Other factors that could contribute to the prediction errors could be variations between calibration and validation samples, e.g. pressure applied during grinding, homogenization, freezing and thawing. Overall, further calibration development is advantageous, particularly with respect to robustification of HYP and protein models.

Another source of error for in-line measurements could be the challenging measurement conditions. For example the reduced exposure time led to reduced SNR (ca.30) compared to the calibration and laboratory validation spectra (ca.50). This might be another reason why the corrected prediction errors were higher for the in-line measurements. Secondly, the large variations in working distance could possibly contribute with errors, depending on the robustness of the pre-processing. It was assumed that the sapphire normalization could handle the variations present in exposure times and working distances, which could not be completely confirmed. After pre-processing, the intensities were lower for the in-line spectra compared to the calibration spectra (Fig. 4b) Although this could be expected due to the more extreme samples in the calibration set, the full extent of the intensity differences might not be justified by the differences in chemistry (i.e. 2%–37% fat in calibration compared to 12%–31% fat for validation samples). This could be indicative of a pre-processing issue or an issue with calibration transfer from laboratory (room temp) to hydrolysis facility (6–8 °C). Notably, the temperatures at the hydrolysis facility were lower than the listed operating temperature (15–33 °C) for the instrument. In the future, it is of interest to look into robustification of the pre-processing as well as exploring if more custom pre-processing for different analytes could be advantageous.

4. Future potential

We have demonstrated that WAI Raman spectroscopy has potential as a tool for characterization of very heterogeneous streams of raw material, in an in-line industrial environment. It is well known that chemical variations in the raw material qualities (e.g. fat-, protein- or collagen content) will significantly affect end-product qualities [1]. Thus, in-line characterisation of raw material qualities could potentially be used to dictate process adjustments (such as enzyme dose, water addition or reaction time), in order to maintain stable product quality over time. Moreover, although the current study focuses on poultry rest raw materials, this indicates that there are many other prospective in-line applications in the food industry. Today, inline sensor systems in the food industry mainly employ NIRS. Such systems have the advantage that they are cheaper, have relatively simple assembly in the process-line, are insensitive to ambient light and have much better sample coverage. In contrast, Raman spectroscopy based systems will require more careful development of practical measurement setup. For instance, one might need shielding from ambient light. However, it is well known that Raman spectroscopy provides a more detailed chemical fingerprint than NIRS, which suggests that WAI Raman spectroscopy in some applications could potentially target more detailed chemistry and quality parameters. We have recently shown this both for fatty acid composition in salmon [11] and for collagen content in ground meat and poultry by-products [4]. Due to the more unique Raman fingerprints compared to NIRS, Raman spectroscopy might also be more robust with respect to variations in absorption and scattering properties within a sample or between samples and has a lower degree of dependence on conserved correlations with other compounds. This means that Raman based models can potentially be more easily maintained in the industry. Overall, WAI Raman spectroscopy may be a good alternative for industrial food quality monitoring, and it is worth considering in cases where NIRS cannot measure all relevant parameters or requires very frequent calibration maintenance. Comparative studies on relevant processes will be needed to verify this.

5. Conclusion

In this work, the cross validated calibration set showed that moderate variations in working distance (6–12 cm) or probe tilt (0, 30°) did

not significantly affect the performance of fat, protein, ash and hydroxyproline estimation for poultry rest raw material. The in-line test of the acquired models represented demanding measurement conditions, including light pollution, large variations in working distance and variations in exposure time. Even so, reasonable variations in average trends of raw material composition were predicted. It is the authors' impression that with further efforts in calibration development, potentially in combination with development of practical measurement setup, the use of Raman spectroscopy as a process control tool in the hydrolysis of poultry rest raw materials is within reach.

Credit author statement

Tiril Aurora Lintvedt: Methodology, Formal analysis, Investigation, Data curation, Writing – original draft, Visualization. **Petter Vejle Andersen**: Methodology, Investigation, Writing – review & editing. **Nils Kristian Afseth**: Conceptualization, Methodology, Writing – review & editing, Supervision. **Jens Petter Wold**: Conceptualization, Methodology, Writing – review & editing, Supervision.

Funding

This work was partially funded by the Research Council of Norway through the projects SFI Digital Food Quality and the Food Pilot Plant [grant numbers 309259, 296083]; along with the Norwegian Agricultural Food Research Foundation through the project Precision Food Production [grant number 314111].

Declaration of competing interest

The authors declare the following financial interests/personal relationships which may be considered as potential competing interests: Tiril Aurora Lintvedt reports equipment, drugs, or supplies was provided by MarqMetrix Inc.

Data availability

Data will be made available on request.

Acknowledgements

We would like to express a special thanks to MarqMetrix Inc. for providing Raman instrumentation through the partnership in the SFI Digital Food Quality project. We would like to extend our sincere thanks to the operations manager Jonathan Fjällman and the operators at Bioco (Hærland, Norway) for making in-line testing of Raman measurements possible. We also extend our thanks to Katinka Dankel, Lene Øverby, Ulrike Böcker and Erik Tengstrand at Nofima for assistance during sample preparation and data acquisition.

Appendix A. Supplementary data

Supplementary data to this article can be found online at https://doi.org/10.1016/j.talanta.2023.125079.

Appendix A. Sample variation

Table A.2
The sample design for the calibration set, made from raw material A-H. One sample part was defined as 1 dl of the respective material.

Sample number	Part 1/6	Part 2/6	Part 3/6	Part 4/6	Part 5/6	Part 6/6
1	A	A	A	A	A	A
2	B	B	B	B	B	B
3	C	C	C	C	C	C
4	D	D	D	D	D	D
5	E	E	E	E	E	E
6	F	F	F	F	F	F
7	G	G	G	G	G	G
8	H	H	H	H	H	H
9	A	A	C	E	F	G
10	D	D	D	F	F	F
11	E	E	G	G	G	G
12	F	F	G	G	G	G
13	C	C	C	C	C	F
14	E	F	F	F	F	F
15	D	E	E	E	E	F
16	F	G	G	G	G	G
17	A	B	E	E	E	G
18	D	D	D	D	D	F
19	D	D	D	D	F	F
20	B	B	C	G	G	G
21	B	B	B	C	C	C
22	C	C	C	C	F	F
23	F	F	F	F	G	G
24	F	F	F	G	G	G
25	B	B	B	E	G	G
26	D	D	D	D	G	G
27	A	B	B	B	D	D
28	B	C	F	G	G	G
29	B	C	F	F	F	F
30	C	F	F	F	F	F
31	C	D	E	E	E	F
32	A	C	C	E	E	E
33	C	C	C	E	F	G
34	E	E	E	F	G	G

(*continued on next page*)

Table A.2 (*continued*)

Sample number	Part 1/6	Part 2/6	Part 3/6	Part 4/6	Part 5/6	Part 6/6
35	B	C	F	F	G	G
36	B	B	B	B	C	F
37	B	C	C	F	F	F
38	C	E	E	E	E	E
39	C	C	C	G	G	G
40	D	E	E	E	F	F
41	D	E	E	E	G	G
42	C	C	D	E	F	F
43	D	E	G	G	G	G
44	B	D	E	F	G	H
45	F	F	F	F	H	H
46	B	B	B	G	H	H
47	C	C	C	F	H	H
48	C	E	E	F	H	H
49	A	A	E	E	E	H

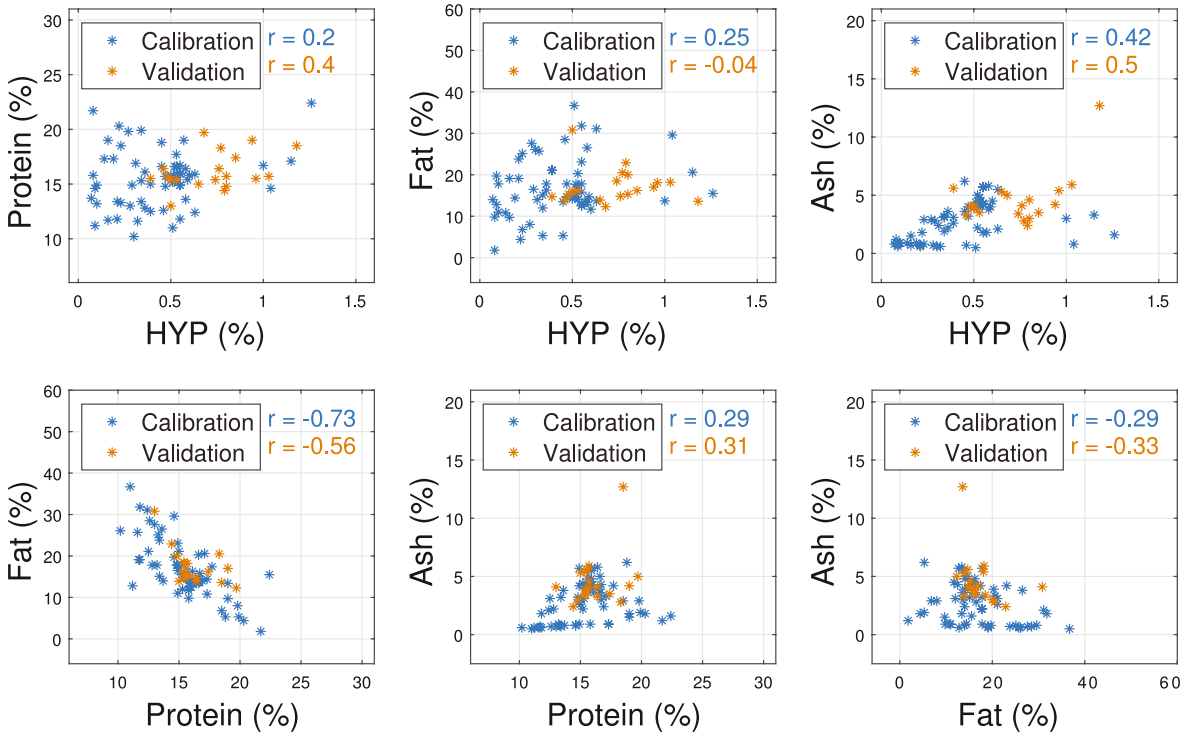

Fig. A.7. Variation in analytes and their correlation in the calibration set compared to in-line validation set.

Appendix B. Background spectrum

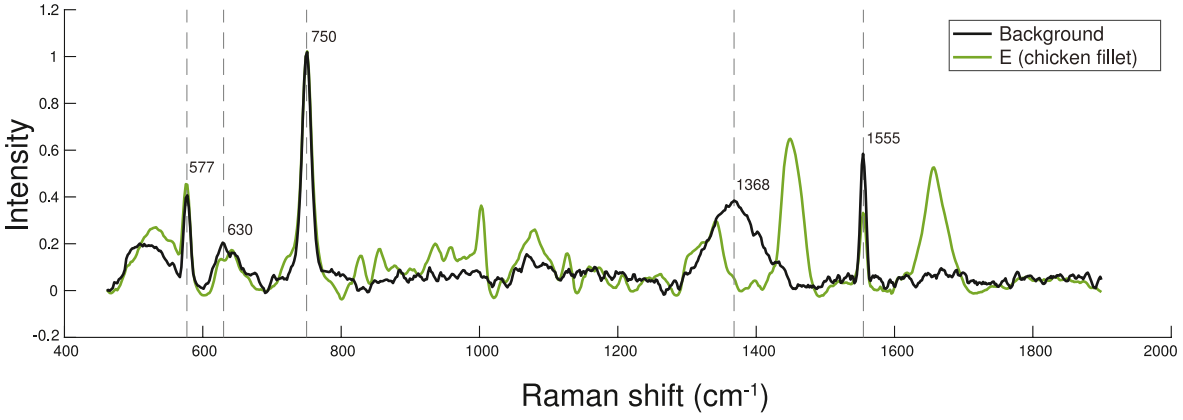

Fig. B.8. Background spectrum, with main spectral features marked (dashed lines). The background spectrum contains signals from the sapphire in the optics, other instrumental components and oxygen. For comparison, the spectrum from the protein-rich material E (chicken fillet) is also included. The spectra are baseline

corrected and normalized by the 750 cm^{-1} sapphire peak intensity for the ease of comparison.

Appendix C. In-line measurements

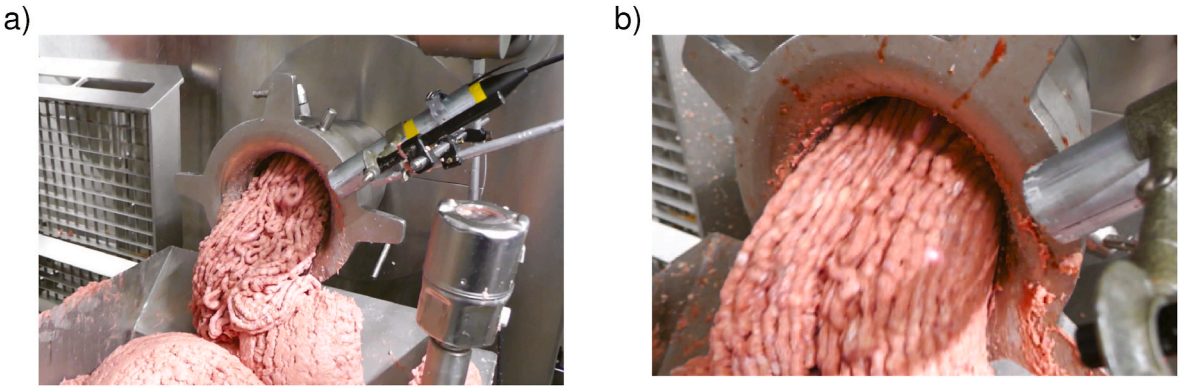

Fig. C.9. Photos of the in-line measurement setup (a,b) at the hydrolysis facility.

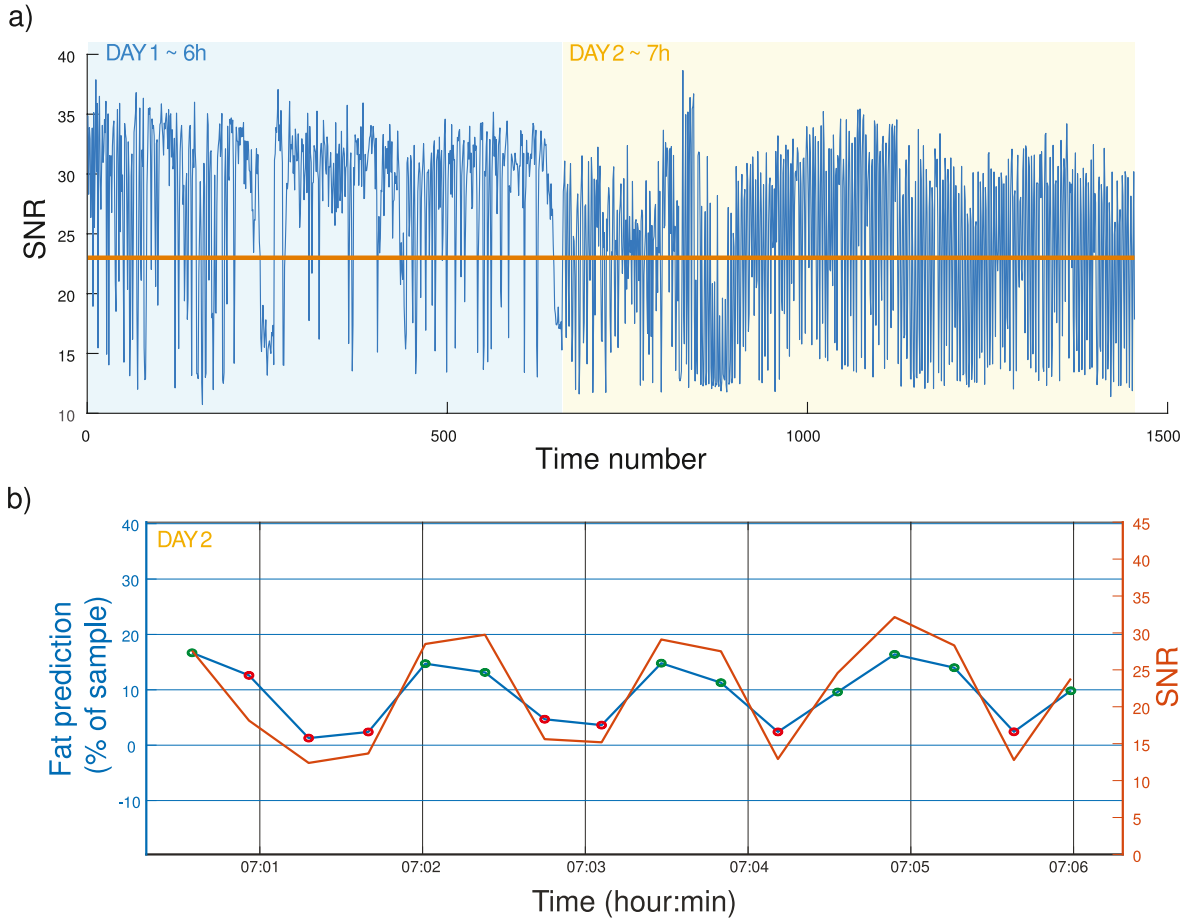

Fig. C.10. Variation in SNR over time, with the threshold used to filter out low quality spectra indicated (a). An example of how fat predictions and SNR alternated within a shorter time span is shown (b). There were clearly periodic variations which corresponded with the alternating output volume (i.e. working distance) at the grinder. Predictions associated with discarded predictions are marked (red), while predictions based on spectra with accepted quality are marked (green).

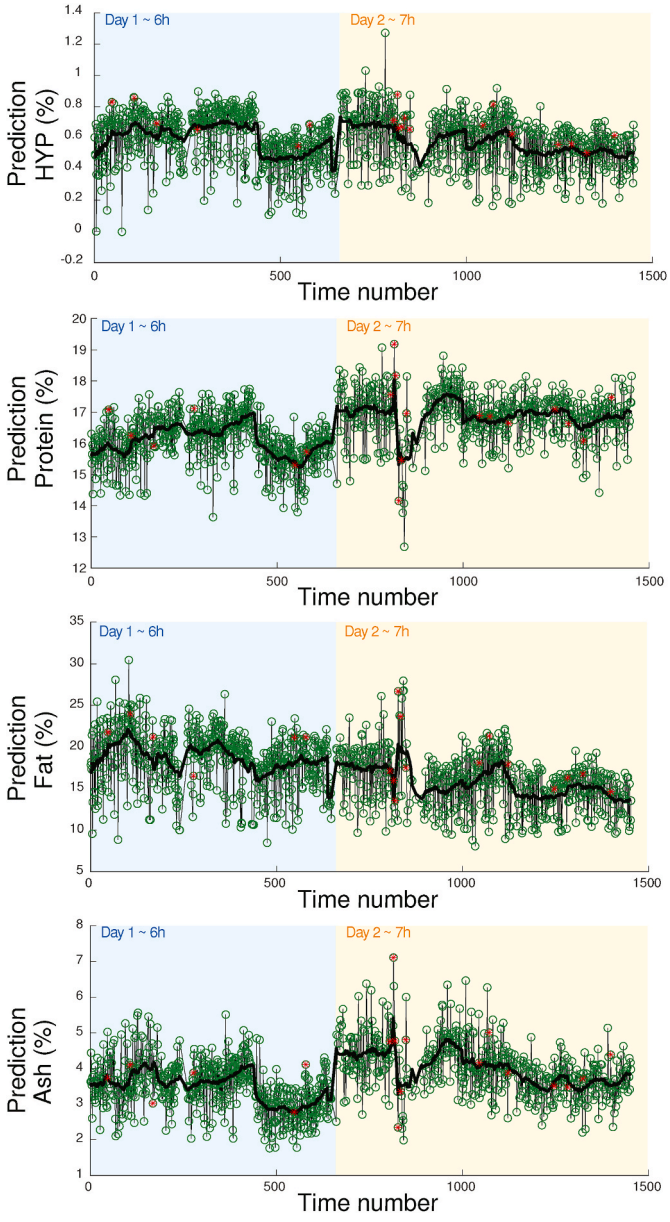

Fig. C.11. All in-line predictions based on spectra with accepted quality. Times for reference sampling and corresponding predictions are marked (red *). The black lines show the average trends, calculated as a 15 min moving average.

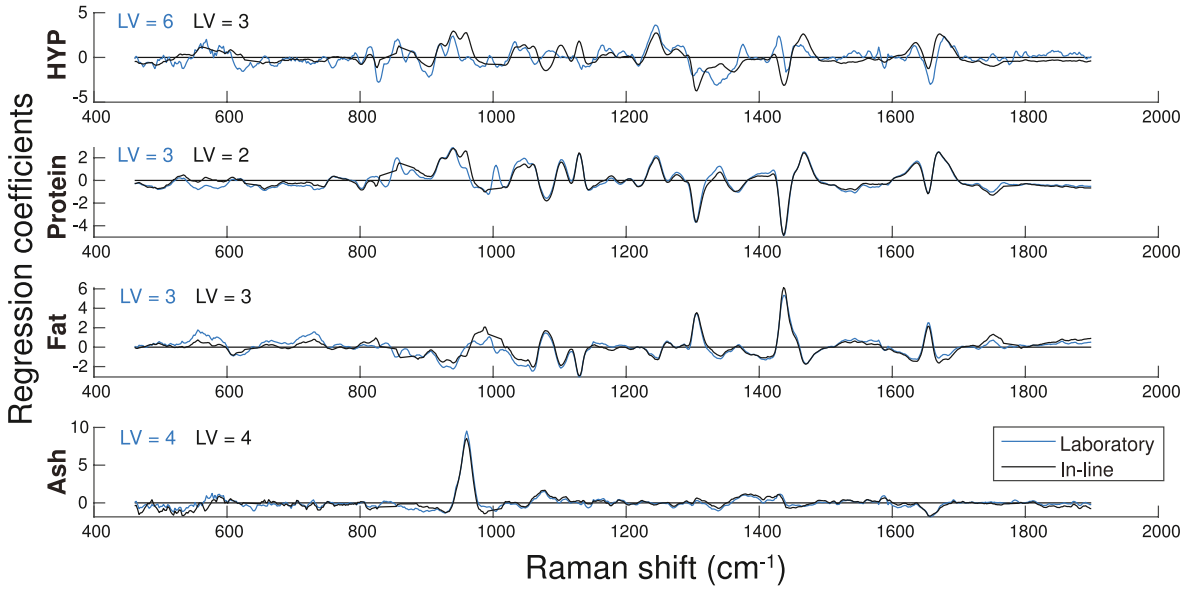

Fig. C.12. Regression coefficients used for the validation, based on in-line measurements (black) and laboratory measurements (blue). The number of latent variables (LV) employed in the respective PLSR models is indicated.

References

[1] D. Lindberg, K.A. Kristoffersen, H. de Vogel-van den Bosch, S.G. Wubshet, U. Böcker, A. Rieder, E. Fricke, N.K. Afseth, Effects of poultry raw material variation and choice of protease on protein hydrolysate quality, Process Biochem. 110 (2021) 85–93, https://doi.org/10.1016/j.procbio.2021.07.014.

[2] D. Lindberg, K.A. Kristoffersen, S.G. Wubshet, L.M.G. Hunnes, M. Dalsnes, K. R. Dankel, V. Høst, N.K. Afseth, Exploring effects of protease choice and protease combinations in enzymatic protein hydrolysis of poultry by-products, Molecules 26 (17) (2021) 5280, https://doi.org/10.3390/molecules26175280.

[3] S.G. Wubshet, J.P. Wold, N.K. Afseth, U. Böcker, D. Lindberg, F.N. Ihunegbo, I. Måge, Feed-forward prediction of product qualities in enzymatic protein hydrolysis of poultry by-products: a spectroscopic approach, Food Bioprocess Technol. 11 (2018) 2032–2043, https://doi.org/10.1007/s11947-018-2161-y.

[4] O. Monago-Maraña, J.P. Wold, R. Rødbotten, K.R. Dankel, N.K. Afseth, Raman, near-infrared and fluorescence spectroscopy for determination of collagen content in ground meat and poultry by-products, Food Sci. Technol. 95 (2019) 267–273, https://doi.org/10.1016/j.lwt.2020.110592.

[5] Y. Dixit, M.P. Casado-Gavalda, R. Cama-Moncunill, P.J. Cullen, C. Sullivan, Challenges in model development for meat composition using multipoint NIR spectroscopy from at-line to in-line monitoring, J. Food Sci. 82 (7) (2017) 1557–1562, https://doi.org/10.1111/1750-3841.13770.

[6] P. Mishra, R. Klont, T. Verkleij, S. Wisse, Translating near-infrared spectroscopy from laboratory to commercial slaughterhouse: existing challenges and solutions, Infrared Phys. Technol. 119 (2021), 103918, https://doi.org/10.1016/j.infrared.2021.103918.

[7] P.V. Andersen, J.P. Wold, N.K. Afseth, Assessment of bulk composition of heterogeneous food matrices using Raman spectroscopy, Appl. Spectrosc. 75 (10) (2021) 1278–1287, https://doi.org/10.1177/00037028211006150.

[8] S.G. Wubshet, J.P. Wold, U. Böcker, K.W. Sanden, N.K. Afseth, Raman spectroscopy for quantification of residual calcium and total ash in mechanically deboned chicken meat, Food Control 95 (2019) 267–273, https://doi.org/10.1016/j.foodcont.2018.08.017.

[9] T.A. Lintvedt, P.V. Andersen, N.K. Afseth, B. Marquardt, L. Gidskehaug, J.P. Wold, Feasibility of in-line Raman spectroscopy for quality assessment in food industry - how fast can we go? Appl. Spectrosc. 76 (5) (2022) 559–568, https://doi.org/10.1177/00037028211056931.

[10] T.A. Lintvedt, P.V. Andersen, N.K. Afseth, K. Heia, S.-K. Lindberg, J.P. Wold, Raman spectroscopy and NIR hyperspectral imaging for in-line estimation of fatty acid features in salmon fillets, Talanta 254 (2023), 124113, https://doi.org/10.1016/j.talanta.2022.124113.

[11] N.K. Afseth, K. Dankel, P.V. Andersen, G.F. Difford, S.S. Horn, A. Sonesson, B. Hillestad, J.P. Wold, E. Tengstrand, Raman and near infrared spectroscopy for quantification of fatty acids in muscle tissue: a salmon case study, Foods 11 (7) (2022) 962, https://doi.org/10.3390/foods11070962.

[12] K. Shin, H. Chung, Wide area coverage Raman spectroscopy for reliable quantitative analysis and its applications, Analyst 138 (12) (2013) 3335–3346, https://doi.org/10.1039/c3an36843b.

[13] H. Wikström, I.R. Lewis, L.S. Taylor, Comparison of sampling techniques for in-line monitoring using Raman spectroscopy, Appl. Spectrosc. 59 (7) (2005) 934–941, https://doi.org/10.1366/0003702054411553.

[14] I. Latka, S. Dochow, C. Krafft, B. Dietzek, J. Popp, Fiber optic probes for linear and nonlinear Raman applications - current trends and future development, Laser Photon. Rev. 7 (5) (2013) 698–731, https://doi.org/10.1002/lpor.201200049.

[15] A. Savitzky, M.J. Golay, Smoothing and differentiation of data by simplified least squares procedures, Anal. Chem. 36 (8) (1964) 1627–1639, https://doi.org/10.1021/ac60214a047.

[16] P.H. Eilers, H.F. Boelens, A perfect smoother, Life Sci. 75 (14) (2003) 3631–3636, https://doi.org/10.1021/ac034173t.

[17] K.H. Liland, T. Almøy, B.H. Mevik, Optimal choice of baseline correction for multivariate calibration of spectra, Appl. Spectrosc. 64 (9) (2010) 1007–1016, https://doi.org/10.1366/000370210792434350.

[18] H. Martens, T. Næs, Multivariate Calibration, second ed., Wiley, Chichester, UK, 1989.

[19] Å. Björck, U.G. Indahl, Fast and stable partial least squares modelling: a benchmark study with theoretical comments, J. Chemom. 31 (8) (2017), e2898 doi:10.1002/cem.2898. URL, https://onlinelibrary.wiley.com/doi/10.1002/cem.2898.

[20] U.G. Indahl, T. Næs, Evaluation of alternative spectral feature extraction methods of textural images for multivariate modelling, J. Chemom. 12 (4) (1998) 261–278, https://doi.org/10.1002/(SICI)1099-128X(199807/08)12:4<261::AID-CEM513>3.3.CO;2-Q.

[21] F. Westad, H. Martens, Variable selection in near infrared spectroscopy based on significance testing in partial least squares regression, J. Near Infrared Spectrosc. 8 (2) (2000) 117–124, https://doi.org/10.1255/jnirs.271.

[22] S. Guo, C. Beleites, U. Neugebauer, S. Abalde-Cela, N.K. Afseth, F. Alsamad, S. Anand, C. Araujo-Andrade, S. Aškrabić, E. Avci, M. Baia, M. Baranska, E. Baria, L.A. Batista de Carvalho, P. de Bettignies, A. Bonifacio, F. Bonnier, E.M. Brauchle, H.J. Byrne, I. Chourpa, R. Cicchi, F. Cuisinier, M. Culha, M. Dahms, C. David, L. Duponchel, S. Duraipandian, S.F. El-Mashtoly, D.I. Ellis, G. Eppe, G. Falgayrac, O. Gamulin, B. Gardner, P. Gardner, K. Gerwert, E.J. Giamarellos-Bourboulis, S. Gizurarson, M. Gnyba, R. Goodacre, P. Grysan, O. Guntinas-Lichius, H. Helgadottir, V.M. Grošev, C. Kendall, R. Kiselev, M. Kölbach, C. Krafft, S. Krishnamoorthy, P. Kubryck, B. Lendl, P. Loza-Alvarez, F.M. Lyng, S. Machill, C. Malherbe, M. Marro, M.P.M. Marques, E. Matuszyk, C.F. Morasso, M. Moreau, H. Muhamadali, V. Mussi, I. Notingher, M.Z. Pacia, F.S. Pavone, G. Penel, D. Petersen, O. Piot, J.V. Rau, M. Richter, M.K. Rybarczyk, H. Salehi, K. Schenke-Layland, S. Schlücker, M. Schosserer, K. Schütze, V. Sergo, F. Sinjab, J. Smulko, G. D. Sockalingum, C. Stiebing, N. Stone, V. Untereiner, R. Vanna, K. Wieland, J. Popp, T. Bocklitz, Comparability of Raman spectroscopic configurations: a large scale cross-laboratory study, Anal. Chem. 92 (24) (2020) 15745–15756, https://doi.org/10.1021/acs.analchem.0c02696.

[23] N.K. Afseth, J.P. Wold, V.H. Segtnan, The potential of Raman spectroscopy for characterisation of the fatty acid unsaturation of salmon, Anal. Chim. Acta 572 (1) (2006) 85–92, https://doi.org/10.1016/j.aca.2006.05.013.

[24] J.R. Beattie, S.E. Bell, C. Borgaard, A. Fearon, B.W. Moss, Prediction of adipose tissue composition using Raman spectroscopy: average properties and individual

fatty acids, Lipids 41 (3) (2006) 287–294, https://doi.org/10.1007/s11745-006-5099-1.
[25] A. Rygula, K. Majzner, K. Marzec, A. Kaczor, M. Pilarczyk, M. Baranska, Raman spectroscopy of proteins: a review, J. Raman Spectrosc. 44 (8) (2013) 1061–1076, https://doi.org/10.1002/jrs.4335.
[26] J.P. Wold, M. O'Farrell, M. Høy, J. Tschudi, On-line determination and control of fat content in batches of beef trimmings by NIR imaging spectroscopy, Meat Sci. 89 (3) (2011) 317–324, https://doi.org/10.1016/j.meatsci.2011.05.001.